Magnetic and transport properties of $Sb_{2-x}Fe_xTe_3$ ($0<x<0.02$) single crystals

Zhenhua Zhou[a)]
Department of Physics, University of Michigan, Ann Arbor, Michigan 48109

Marek Žabèík and Petr Lošták
Faculty of Chemical Technology, University of Pardubice, 532 10 Pardubice, Czech Republic

Ctirad Uher
Department of Physics, University of Michigan, Ann Arbor, Michigan 48109

(Received 19 April 2005; accepted 10 January 2006; published online 16 February 2006)

Magnetization, electrical resistivity, and Hall coefficient of single crystals $Sb_{2-x}Fe_xTe_3$ ($0<x<0.02$) have been measured from 2 to 300 K. Doping diamagnetic Sb_2Te_3 with Fe results in a paramagnetic behavior and the exchange interaction between Fe ions is determined to be antiferromagnetic based on low-temperature magnetization investigations. We detect no presence of a ferromagnetic ordering in Fe-doped Sb_2Te_3 down to 2 K. Fe doping initially increases the concentration of holes in relation to the case of pure Sb_2Te_3 but it rapidly saturates. The electrical resistivity increases throughout the temperature range studied on account of enhanced carrier scattering. © *2006 American Institute of Physics*. [DOI: 10.1063/1.2171787]

I. INTRODUCTION

Antimony telluride (Sb_2Te_3) is a narrow-band-gap semiconductor ($E_g \sim 0.26$ eV around room temperature) with the tetradymite structure (space group $R\bar{3}m-D_{3d}^5$) composed of repeated planes of five-atomic layer lamellas separated by a van der Waals gap.[1] As grown, undoped Sb_2Te_3 has a rather large concentration of holes around 10^{20} cm^{-3} due to the presence of native antisite defects (Sb atoms occupying Te lattice sites)[2–5] and is diamagnetic.[6]

Recently, considerable interest has been stimulated by the influence of transition-metal dopants on magnetic and transport properties of Sb_2Te_3.[7–14] Among the noteworthy findings is the observation of a long-range magnetic ordering that develops in vanadium- and chromium-doped Sb_2Te_3 at low temperatures.[11,12] The indirect exchange interaction mediated by the free charge carriers (holes) between the vanadium and chromium ions embedded in the Sb sublattice gives rise to ferromagnetism with the Curie temperature in excess of 20 K. Thus, the structures represent bulk, diluted magnetic semiconductors (DMS) in the sense that the matrix is a highly anisotropic, octahedrally bonded environment with the magnetic ions other than Mn. In fact, attempts to dope crystals of Sb_2Te_3 with Mn ions have invariably failed to produce a ferromagnetic state even though the structure was able to accommodate a significant (4.5%) concentration of Mn ions.[13] The sister compound, Bi_2Te_3, was shown recently to support ferromagnetism below 12 K when Fe ions were introduced into the lattice.[15] It is therefore of interest to investigate whether Fe might stimulate ferromagnetism also in Sb_2Te_3.

[a)]Electronic mail: zzh@umich.edu

II. EXPERIMENTAL PROCEDURE

Single crystals of $Sb_{2-x}Fe_xTe_3$ ($x=0$, 0.0083, 0.0177, 0.0190) were grown using the Bridgman method starting with high-purity Sb, Fe, and Te elements. Samples in the form of rectangles with typical dimensions of $1.0\times2.5\times5$ mm^3 were cut for measurements of magnetic and transport properties. The actual Fe content was determined using electron microprobe analysis. Magnetization measurements were done in a Quantum Design superconducting quantum interference device-based magnetometer equipped with a 5.5 T magnet. Transport properties (electrical resistivity and Hall effect) were carried out with the aid of a low-frequency (16 Hz) Linear Research ac bridge over the temperature range of 2–300 K. Leads to the sample were fine copper wires (25 μm in diameter) attached with indium.

III. RESULTS AND DISCUSSIONS

A. Magnetic properties

When a magnetic field is applied, Sb_2Te_3 single crystal shows a diamagnetic behavior with a typical magnetic susceptibility $\chi_0=-3.8\times10^{-7}$ emu/(g Oe).[11] It is worthwhile to note that the value of this susceptibility may vary somewhat from sample to sample. This variation is not surprising since the total susceptibility of Sb_2Te_3 single crystals is composed of contributions arising from both the Sb_2Te_3 matrix and the free carriers that are present due to antisite defects. A significant amount of free charge carriers in Sb_2Te_3 single crystals can result in a positive Pauli paramagnetism which is described by its susceptibility $\chi_{\text{Pauli}}=\mu_B{}^2D(E_F)$. Here μ_B is the Bohr magneton and $D(E_F)$ is the carrier density of states at the Fermi level. While the contribution from the Sb_2Te_3 matrix can be considered to be constant, the contribution from the carriers strongly depends on the effective mass and on their concentration.

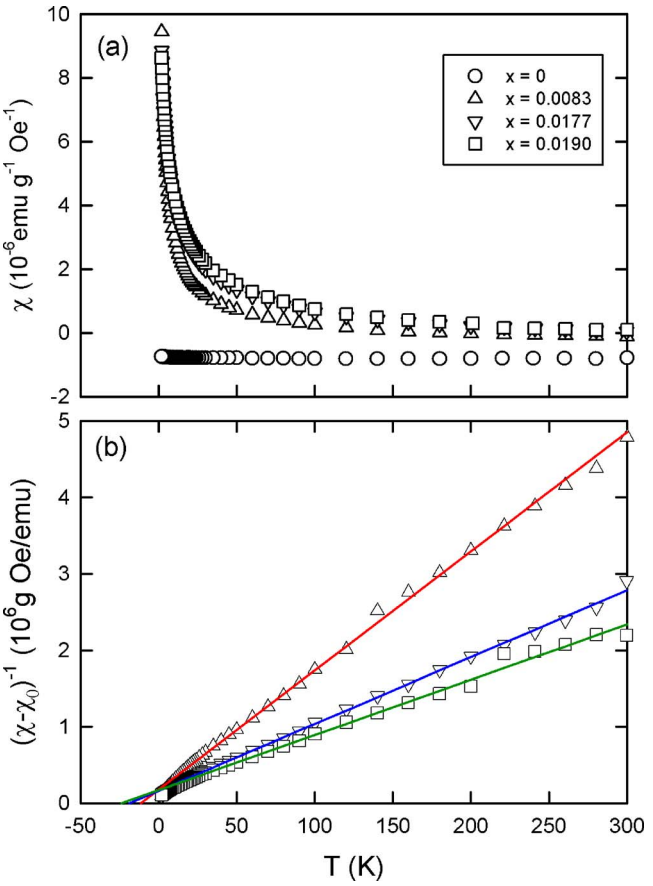

FIG. 1. (a) Magnetic susceptibility vs temperature for $Sb_{2-x}Fe_xTe_3$ samples. (b) Inverse magnetic susceptibilities as a function of temperature for $Sb_{2-x}Fe_xTe_3$ single crystals. The straight lines are the Curie-Weiss fitting of the high-temperature susceptibility data and indicate a negative paramagnetic Curie temperature for all three $Sb_{2-x}Fe_xTe_3$ samples.

Iron enters the structure in the form of ions that substitute on the Sb sublattice[14] and makes Sb_2Te_3 a paramagnetic material. Figure 1(a) shows the magnetic susceptibility χ of $Sb_{2-x}Fe_xTe_3$ samples plotted as a function of temperature and obtained in a magnetic field of 1000 Oe applied parallel to the c axis of the crystal. While the magnetic susceptibility of undoped Sb_2Te_3 is constant throughout the temperature range from 300 to 2 K, the susceptibility of all three $Sb_{2-x}Fe_xTe_3$ samples increases with decreasing temperature. Figure 1(b) depicts the inverse susceptibility $(\chi-\chi_0)^{-1}$ vs T for the same $Sb_{2-x}Fe_xTe_3$ samples. The linear dependence of $(\chi-\chi_0)^{-1}$ on T at high temperatures is apparent. The high-temperature region (from 50 to 300 K) of the inverse magnetic susceptibility was used to fit the Curie-Weiss law of the form

$$\chi(T) = \frac{C}{T-\theta_{CW}} + \chi_0, \tag{1}$$

where C is the Curie constant, θ_{CW} is the paramagnetic Curie temperature, and χ_0 is the temperature-independent contribution from the Sb_2Te_3 matrix and free carriers (holes in the present system). The fitted values are listed in Table I, and the fits are shown by solid curves in Fig. 1(b). The extrapolation of high-temperature $(\chi-\chi_0)^{-1}$ data intersects the temperature axis at negative temperature values, indicating negative paramagnetic Curie temperatures for all three samples. The paramagnetic Curie temperatures are determined as -11.5, -18.8, and -23.9 K for the samples with $x=0.0083$, 0.0177, and 0.0190, respectively. Both C and $-\theta_{CW}$ increase nearly linearly with the increasing Fe-ion concentration. We detect no tendency of forming ferromagnetic ordering down to at least 2 K, unlike the case of Fe doping in Bi_2Te_3 where ferromagnetism sets in below about 12 K.[15] The negative paramagnetic Curie temperatures suggest the presence of antiferromagnetic coupling of Fe ions in $Sb_{2-x}Fe_xTe_3$. Clearly, $(\chi-\chi_0)^{-1}$ curves at low temperatures deviate from straight lines. This may be due to a contribution from stronger antiferromagnetic interactions between Fe ions at low temperatures.

Calculations of the effective Bohr magneton number p_{eff} are made via the equation $C=N\,p_{eff}^2\mu_B^2/3k_B$, where N is the concentration of Fe ions obtained from the electron microprobe results, μ_B is the Bohr magneton, and k_B is the Boltzmann constant. Values of the spin per Fe ion, S, were calculated from $p_{eff}=g\sqrt{J(J+1)}$ taking the Landé g factor equal $g=2$ and the angular momentum quantum number $J=L+S \approx S$ (orbital angular momentum is assumed quenched due to the crystal field of neighboring atoms). The calculated spin-only values of S of all three samples are close to 2.5. That suggests that the valence state of iron in the $Sb_{2-x}Fe_xTe_3$ crystals is Fe^{3+} and all five electrons of Fe^{3+} are in the high spin state.

To gain more insight into the nature of the magnetic state of $Sb_{2-x}Fe_xTe_3$ samples, we performed low-temperature magnetization studies in the field of up to 5 T. In all three Fe-doped samples the magnetization increases with increasing magnetic field but no hysteresis loop is observed upon cycling the magnetic field. The low-temperature magnetization curves are plotted in Figs. 2(a)–2(c) after the diamagnetic contribution $\chi_0 H$ was subtracted. The Brillouin function with $J=5/2$, defined by

TABLE I. Lists of Fe concentration (C_{Fe}), concentration of holes (p) and their mobility (μ) at 300 K, and fitting parameters of the Curie-Weiss analysis of $Sb_{2-x}Fe_xTe_3$: C is the Curie constant, θ_{CW} is the paramagnetic Curie temperature, χ_0 is the temperature-independent diamagnetic contribution from the host crystal, p_{eff} is the effective Bohr magneton number per iron ion, and S is the spin quantum number assuming that orbital angular momentum is quenched.

x	C_{Fe}(cm^{-3})	p(cm^{-3})	μ(cm^2/V s)	C[emu K/(g Oe)]	$\theta_{CW}(K)$	χ_0(emu g^{-1} Oe^{-1})	p_{eff}	S
0	⋯	8.82×10^{19}	338	⋯	⋯	-3.8×10^{-7}	⋯	⋯
0.0083	5.25×10^{19}	3.13×10^{20}	83	6.421×10^{-5}	−11.5	-3.222×10^{-7}	6.19	2.6
0.0177	1.12×10^{20}	1.80×10^{20}	96	1.144×10^{-4}	−18.8	-3.016×10^{-7}	5.66	2.4
0.0190	1.20×10^{20}	2.10×10^{20}	87	1.385×10^{-4}	−23.9	-3.591×10^{-7}	6.01	2.5

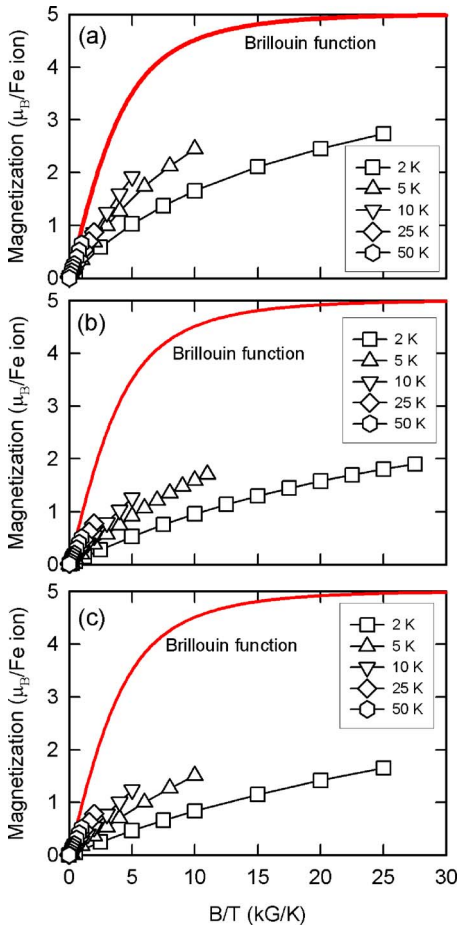

FIG. 2. Magnetization of single crystals (a) $Sb_{1.9917}Fe_{0.0083}Te_3$, (b) $Sb_{1.9823}Fe_{0.0177}Te_3$, and (c) $Sb_{1.9810}Fe_{0.0190}Te_3$ at low temperatures plotted as a function of B/T. The solid lines are the Brillouin function curve assuming $J=5/2$.

$$B_J(x) = \frac{2J+1}{2J}\coth\left[\frac{(2J+1)x}{2J}\right] - \frac{1}{2J}\coth\left(\frac{x}{2J}\right), \qquad (2)$$

is also plotted as the heavy solid lines for comparison. Here $x=gJ\mu_B B/k_B T$. As Figs. 2(a)–2(c) indicate, the low-temperature magnetization curves of all three Fe-doped samples are much smaller than the Brillouin function prediction. The difference between the Brillouin function prediction and the experimental values becomes smaller as the temperature increases. This again suggests that the low-temperature magnetization in $Sb_{2-x}Fe_xTe_3$ crystals does not come solely from isolated Fe ions.

It is likely that the low-temperature magnetization is modified by interactions between the ions of Fe. Although we assume a homogeneous distribution of Fe throughout the Sb_2Te_3 matrix and, at these dilute concentrations, Fe ions indeed should be spaced far apart from each other, this need not be strictly so in the actual crystal. There might be regions where Fe ions on the Sb sublattice are more closely spaced giving rise to Fe–Fe interactions. Taking such interactions into account, the overall magnetization $M(T)$, after subtracting the diamagnetic contribution due to the Sb_2Te_3 matrix, can be written as

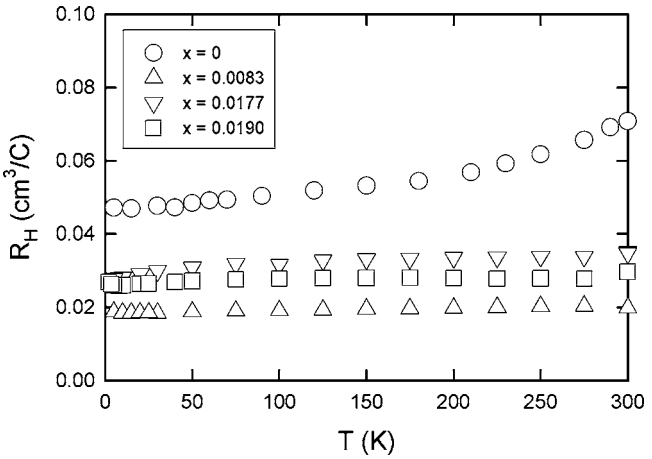

FIG. 3. Hall coefficient as a function of temperature for $Sb_{2-x}Fe_xTe_3$ samples. The current is perpendicular to the c axis and the magnetic field is parallel to the c axis.

$$M(T) = M_{\mathrm{Fe}}(T) + M_{\mathrm{Fe-Fe}}(T). \qquad (3)$$

Here, $M_{\mathrm{Fe}}(T)$ is the temperature-dependent paramagnetic contribution from isolated Fe^{3+} ions which should conform to the Brillouin function, and $M_{\mathrm{Fe-Fe}}(T)$ is the contribution from the Fe–Fe interactions. This latter contribution is temperature dependent and becomes progressively more important at low temperatures. Based on the data in Figs. 2(a)–2(c) which indicate that, for the same B/T, the experimental values are smaller than those predicted by the Brillouin function, this implies that the contribution $M_{\mathrm{Fe-Fe}}(T)$ is negative for all $Sb_{2-x}Fe_xTe_3$ samples at the temperatures up to 50 K. Therefore, the net exchange interactions between Fe^{3+} ions are of antiferromagnetic nature. Since the difference between the Brillouin function prediction and the experimental values is larger in samples with higher Fe content, this also suggests that the antiferromagnetic Fe–Fe coupling strength increases with the concentration of Fe ions.

B. Transport properties

Figures 3 and 4 show the Hall coefficient R_H (current perpendicular to the c axis, magnetic field parallel to the c

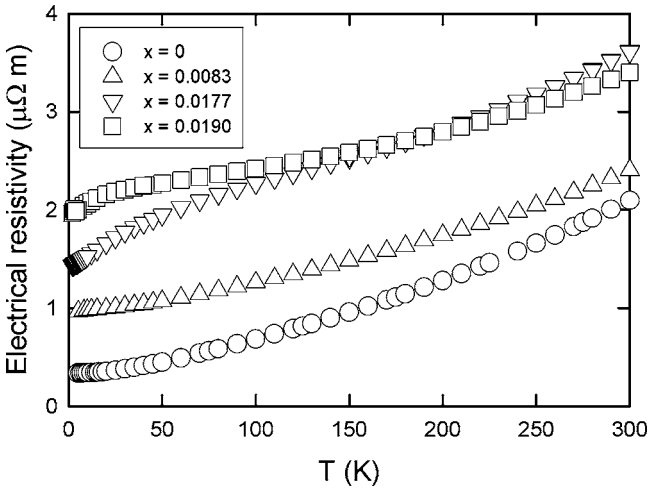

FIG. 4. Electrical resistivity as a function of temperature for $Sb_{2-x}Fe_xTe_3$. The current is perpendicular to the c axis.

axis) and the in-plane electrical resistivity ρ, respectively, of $Sb_{2-x}Fe_xTe_3$ samples from 2 to 300 K. Clearly, the electrical transport is dominated by the conduction of holes and the samples display a metallic conduction (degenerate semiconductors) with the progressively increasing resistivity as the concentration of Fe increases. While the Hall coefficient of pure Sb_2Te_3 shows a notable temperature dependence, the Fe-doped samples display only a very weak effect of temperature. Assuming a single band model, the concentration of holes initially increases as Fe is accommodated in the Sb_2Te_3 crystal lattice. However, at the doping level above $x = 0.0083$, Fe has a much smaller effect on the concentration of holes and perhaps may even decrease their concentration. This observation agrees with the earlier report by Švanda *et al.*,[14] who measured the Hall coefficient at ambient temperature. One should use caution, however, when attempting to extract the actual carrier concentration from the Hall-effect data in the structure such as Sb_2Te_3. The reason is the presence of two valence bands (light-hole and heavy-hole bands) that, depending on the doping, may both be accessible.[16] The hole mobilities in $Sb_{2-x}Fe_xTe_3$ are about a factor of 4 smaller than the corresponding mobility in pure Sb_2Te_3, indicating an enhanced charge-carrier scattering. In view of the 3+ valence state of Fe that comes out of the analysis of magnetic susceptibility data, the initial increase in the density of holes as Fe substitutes on the Sb sublattice (antimony is formally in the Sb^{3+} state) may not arise from a direct doping effect of Fe. Rather, it is likely that the change in the carrier density originates in the interactions of Fe with the native antisite defects. The importance of such interactions has been demonstrated recently in the case of Mn-doped Sb_2Te_3.[17]

IV. CONCLUSIONS

In conclusion, we find that doping the diamagnetic Sb_2Te_3 matrix with Fe results in a paramagnetic solid. There is no hint of ferromagnetism down to 2 K, in contrast to the case of Fe doping in Bi_2Te_3 where ferromagnetism is observed below 12 K. Magnetization data are analyzed assuming contributions from localized Fe ions and Fe–Fe interactions. The results strongly suggest the existence of a net antiferromagnetic coupling between Fe ions and the strength of this coupling increases with decreasing temperature. It is not clear why Fe stimulates ferromagnetism in Bi_2Te_3 and not in Sb_2Te_3 in spite of the latter having an order of magnitude higher density of holes. Perhaps the antiferromagnetic interactions among Fe ions in Sb_2Te_3 are much stronger than those in Bi_2Te_3. However, because a detailed analysis of the valence state of Fe in Bi_2Te_3 was not given in Ref. 15, we lack a direct comparison between the magnetic states of Fe in the Bi_2Te_3 and Sb_2Te_3 lattices. While the electrical resistivity increases with the Fe content, the Hall coefficient and hence the carrier density display a more complicated behavior. It is likely that the Fe ions interact with the antisite defects and this interaction plays a major role in the variation of the charge-carrier (hole) density. Detailed band-structure calculations concerning the influence of Fe in both Sb_2Te_3 and Bi_2Te_3 would be very useful in shedding light on the type and strength of magnetic interactions in these layered compounds.

ACKNOWLEDGMENTS

This work was supported by the National Science Foundation Grant Nos. NSF-INT 0201114 and NSF-DMR 0305221 and by the Ministry of Education of the Czech Republic under Project No. MSM 0021627501.

[1] D. L. Lovett, *Semimetals and Narrow-Band-Gap Semiconductors* (Pion, London, 1977).
[2] N. Kh. Abrikosov, L. V. Poretskaya, and I. P. Ivanova, Zh. Neorg. Khim. **4**, 2525 (1959).
[3] B. Roy, B. R. Chakraborty, R. Bhattacharya, and A. K. Dutta, Solid State Commun. **25**, 617 (1978).
[4] J. Horák, L. Tichý, P. Lošták, and A. Vaško, Cryst. Lattice Defects **6**, 233 (1976).
[5] Y. Kim, A. DiVenere, G. K. L. Wong, J. B. Ketterson, S. Cho, and J. R. Meyer, J. Appl. Phys. **91**, 715 (2002).
[6] J. Horák, M. Matyáš, and L. Tichý, Phys. Status Solidi A **27**, 621 (1975).
[7] P. Lošták, Č. Drašar, I. Klichová, J. Navrátil, and M. Vlček, Cryst. Res. Technol. **32**, 369 (1997).
[8] P. Lošták, Č. Drašar, J. Navrátil, and L. Beneš, Cryst. Res. Technol. **31**, 403 (1996).
[9] Č. Drašar, P. Lošták, J. Navrátil, T. Černohorský, and V. Mach, Phys. Status Solidi B **191**, 523 (1995).
[10] V. A. Kulbachinskii, N. Miura, H. Nakagawa, Č. Drašar, and P. Lošták, J. Phys.: Condens. Matter **11**, 5273 (1999).
[11] J. S. Dyck, P. Hájek, P. Lošták, and C. Uher, Phys. Rev. B **65**, 115212 (2002).
[12] J. S. Dyck, Č. Drašar, P. Lošták, and C. Uher, Phys. Rev. B **71**, 115214 (2005).
[13] J. S. Dyck, P. Švanda, P. Lošták, J. Horák, W. Chen, and C. Uher, J. Appl. Phys. **94**, 7631 (2003).
[14] P. Švanda, P. Lošták, Č. Drašar, J. Navrátil, L. Beneš, and T. Černohorský, Radiat. Eff. Defects Solids **153**, 59 (2000).
[15] V. A. Kulbachinskii, A. Yu. Kaminskii, K. Kindo, Y. Narumi, K. Suga, P. Lošták, and P. Švanda, JETP Lett. **73**, 352 (2001).
[16] V. A. Kulbachinskii *et al.*, Phys. Rev. B **52**, 10915 (1995).
[17] J. Horák, P. Lošták, Č. Drašar, J. S. Dyck, Z. Zhou, and C. Uher, J. Solid State Chem. **178**, 2907 (2005).